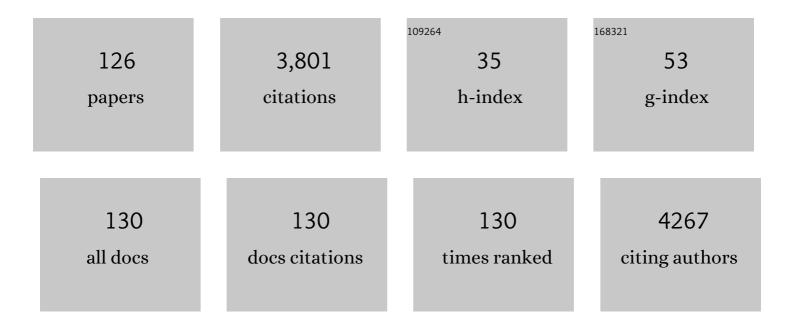


## List of Publications by Year in descending order

Source: https://exaly.com/author-pdf/6036542/publications.pdf Version: 2024-02-01



VAN XII

#	Article	IF	CITATIONS
1	Encapsulation of CH <sub>3</sub> NH <sub>3</sub> PbBr <sub>3</sub> Perovskite Quantum Dots in MOF-5 Microcrystals as a Stable Platform for Temperature and Aqueous Heavy Metal Ion Detection. Inorganic Chemistry, 2018, 57, 4613-4619.	1.9	196
2	A Large 24-Membered-Ring Germanate Zeolite-Type Open-Framework Structure with Three-Dimensional Intersecting Channels. Angewandte Chemie - International Edition, 2001, 40, 2166-2168.	7.2	152
3	Protein adsorption and cell adhesion on cationic, neutral, and anionic 2-methacryloyloxyethyl phosphorylcholine copolymer surfaces. Biomaterials, 2009, 30, 4930-4938.	5.7	141
4	A carbon dot-encapsulated UiO-type metal organic framework as a multifunctional fluorescent sensor for temperature, metal ion and pH detection. Journal of Materials Chemistry C, 2018, 6, 4396-4399.	2.7	102
5	A new MOFs/polymer hybrid membrane: MIL-68(Al)/PVDF, fabrication and application in high-efficient removal of p-nitrophenol and methylene blue. Separation and Purification Technology, 2019, 215, 217-226.	3.9	95
6	Highly safe and ionothermal synthesis of Ti3C2 MXene with expanded interlayer spacing for enhanced lithium storage. Journal of Energy Chemistry, 2020, 47, 203-209.	7.1	91
7	Low-temperature direct bonding of glass nanofluidic chips using a two-step plasma surface activation process. Analytical and Bioanalytical Chemistry, 2012, 402, 1011-1018.	1.9	80
8	Enhanced up-conversion luminescence and optical temperature sensing in graphitic C <sub>3</sub> N <sub>4</sub> quantum dots grafted with BaWO <sub>4</sub> :Yb <sup>3+</sup> ,Er <sup>3+</sup> phosphors. Journal of Materials Chemistry C, 2019, 7, 6112-6119.	2.7	78
9	Polyethyleneimine (PEI) incorporated Cu-BTC composites: Extended applications in ultra-high efficient removal of congo red. Journal of Solid State Chemistry, 2019, 270, 231-241.	1.4	74
10	Dual-Emissive CsPbBr <sub>3</sub> @Eu-BTC Composite for Self-Calibrating Temperature Sensing Application. Crystal Growth and Design, 2020, 20, 454-459.	1.4	70
11	Immobilization of lysozyme proteins on a hierarchical zeolitic imidazolate framework (ZIF-8). Dalton Transactions, 2017, 46, 2114-2121.	1.6	68
12	Zeroâ€Dimensional Luminescent Metal Halide Hybrids Enabling Bulk Transparent Medium as Largeâ€Area Xâ€Ray Scintillators. Advanced Optical Materials, 2022, 10, .	3.6	67
13	Microfluidic flow control on charged phospholipidpolymer interface. Lab on A Chip, 2007, 7, 199-206.	3.1	64
14	Nonenzymatic electrochemical glucose biosensor constructed by NiCo2O4@Ppy nanowires on nickel foam substrate. Sensors and Actuators B: Chemical, 2019, 292, 121-128.	4.0	60
15	Improvement of Methane–Framework Interaction by Controlling Pore Size and Functionality of Pillared MOFs. Inorganic Chemistry, 2017, 56, 2581-2588.	1.9	59
16	Eu <sup>3+</sup> /Tb <sup>3+</sup> functionalized Bi-based metal–organic frameworks toward tunable white-light emission and fluorescence sensing applications. Dalton Transactions, 2018, 47, 16696-16703.	1.6	55
17	Investigation of Extra-Large Pore Zeolite Synthesis by a High-Throughput Approach. Chemistry of Materials, 2011, 23, 4709-4715.	3.2	53
18	A Microfluidic Hydrogel Capable of Cell Preservation without Perfusion Culture under Cellâ€Based Assay Conditions. Advanced Materials, 2010, 22, 3017-3021.	11.1	51

#	Article	IF	CITATIONS
19	Adsorption behavior of Rhodamine B on nanoporous polymers. RSC Advances, 2015, 5, 104915-104922.	1.7	51
20	Fabrication of nobleâ€metalâ€free gâ€C <sub>3</sub> N <sub>4</sub> â€MILâ€53(Fe) composite for enhanced photocatalytic H <sub>2</sub> â€generation performance. Applied Organometallic Chemistry, 2018, 32, e4597.	1.7	49
21	Fabrication of NH2-MIL-125(Ti) incorporated TiO2 nanotube arrays composite anodes for highly efficient PEC water splitting. Separation and Purification Technology, 2019, 228, 115764.	3.9	48
22	Hierarchical Accordion-like Lanthanide-Based Metal–Organic Frameworks: Solvent-Free Syntheses and Ratiometric Luminescence Temperature-Sensing Properties. Crystal Growth and Design, 2019, 19, 6586-6591.	1.4	48
23	Simple synthesis of ZnO nanoflowers and its photocatalytic performances toward the photodegradation of metamitron. Materials Research Bulletin, 2016, 76, 235-239.	2.7	47
24	Marine Biofilms with Significant Corrosion Inhibition Performance by Secreting Extracellular Polymeric Substances. ACS Applied Materials & Interfaces, 2021, 13, 47272-47282.	4.0	47
25	Fabrication of hybrid magnetic HKUST-1 and its highly efficient adsorption performance for Congo red dye. RSC Advances, 2015, 5, 19199-19202.	1.7	46
26	Synthesis and Structure of an Unprecedented Layered Vanadate Complex Containing Double-Helical Chains: [{CollI(phen)2}2V8O23]. European Journal of Inorganic Chemistry, 2004, 2004, 1385-1388.	1.0	45
27	Suppression of Protein Adsorption on a Charged Phospholipid Polymer Interface. Biomacromolecules, 2009, 10, 267-274.	2.6	44
28	A facile strategy for fabricating Agl–MIL-53(Fe) composites: superior interfacial contact and enhanced visible light photocatalytic performance. New Journal of Chemistry, 2018, 42, 3799-3807.	1.4	44
29	Efficient and selective removal of congo red by mesoporous amino-modified MIL-101(Cr) nanoadsorbents. Powder Technology, 2019, 356, 162-169.	2.1	44
30	Trap depth engineering in MgGa2O4: Bi3+ for muticolor dynamic anti-counterfeiting, encryption and optical temperature sensing applications. Chemical Engineering Journal, 2022, 437, 135389.	6.6	43
31	Phospholipid Polymer Biointerfaces for Lab-on-a-Chip Devices. Annals of Biomedical Engineering, 2010, 38, 1938-1953.	1.3	42
32	Microchip-based cellular biochemical systems for practical applications and fundamental research: from microfluidics to nanofluidics. Analytical and Bioanalytical Chemistry, 2012, 402, 99-107.	1.9	41
33	A Gallogermanate Zeolite with Elevenâ€Memberedâ€Ring Channels. Angewandte Chemie - International Edition, 2013, 52, 5501-5503.	7.2	40
34	Coumarin 7 functionalized europium-based metal–organic-framework luminescent composites for dual-mode optical thermometry. Journal of Materials Chemistry C, 2020, 8, 13328-13335.	2.7	39
35	Magnetization of a Cu(II)-1,3,5-benzenetricarboxylate metal-organic framework for efficient solid-phase extraction of Congo Red. Mikrochimica Acta, 2015, 182, 2313-2320.	2.5	38
36	Synthesis, characterization, and photocatalytic degradation properties of ZnO/ZnFe <sub>2</sub> O <sub>4</sub> magnetic heterostructures. New Journal of Chemistry, 2017, 41, 15433-15438.	1.4	36

#	Article	IF	CITATIONS
37	Dopant concentration-dependent morphological evolution of Zn2GeO4:Mn2+/Eu3+ phosphor and optical temperature sensing performance. Journal of Alloys and Compounds, 2019, 770, 149-157.	2.8	36
38	Hierarchical kiwifruit-like ZnO/ZnFe2O4 heterostructure for high-sensitive triethylamine gaseous sensor. Sensors and Actuators B: Chemical, 2021, 344, 130251.	4.0	36
39	Synergistic weak/strong coupling luminescence in Eu-metal-organic framework/Zn2GeO4:Mn2+ nanocomposites for ratiometric luminescence thermometer. Dyes and Pigments, 2018, 157, 321-327.	2.0	35
40	Ag nanoparticle-functionalized ZnO micro-flowers for enhanced photodegradation of herbicide derivatives. Chemical Physics Letters, 2017, 679, 119-126.	1.2	34
41	Surface functionalization of MIL-101(Cr) by aminated mesoporous silica and improved adsorption selectivity toward special metal ions. Dalton Transactions, 2019, 48, 5384-5396.	1.6	33
42	Hierarchical α-Fe2O3 microcubes supported on Ni foam as non-enzymatic glucose sensor. Applied Surface Science, 2020, 512, 145710.	3.1	33
43	Electrodeposition of hydroxyapatite on nickel foam and further modification with conductive polyaniline for non-enzymatic glucose sensing. Electrochimica Acta, 2018, 280, 315-322.	2.6	32
44	Construction of an Aminated MIL-53(Al)-Functionalized Carbon Nanotube for the Efficient Removal of Bisphenol AF and Metribuzin. Inorganic Chemistry, 2020, 59, 2667-2679.	1.9	32
45	Enhanced selective acetone-sensing performance of hierarchical hollow SnO <sub>2</sub> /l̂±-Fe <sub>2</sub> O <sub>3</sub> microcubes. Journal of Materials Chemistry C, 2019, 7, 11984-11990.	2.7	30
46	Fabrication of polyaniline sensitized grey-TiO 2 nanocomposites and enhanced photocatalytic activity. Separation and Purification Technology, 2017, 184, 248-256.	3.9	29
47	In- situ solid-phase fabrication of Ag/AgX (X=Cl, Br, I)/g-C3N4 composites for enhanced visible-light hydrogen evolution. International Journal of Hydrogen Energy, 2019, 44, 21397-21405.	3.8	29
48	Controlled Synthesis of Porous Hierarchical ZnFe <sub>2</sub> O <sub>4</sub> Micro-/Nanostructures with Multifunctional Photocatalytic Performance. Inorganic Chemistry, 2018, 57, 15481-15488.	1.9	28
49	Aminated metalâ€organic framework (NH <sub>2</sub> â€MILâ€101(Cr)) incorporated polyvinylidene (PVDF) hybrid membranes: Synthesis and application in efficient removal of Congo red from aqueous solution. Applied Organometallic Chemistry, 2020, 34, e5281.	1.7	28
50	A facile synthesis of a ZIF-derived ZnS/ZnIn <sub>2</sub> S <sub>4</sub> heterojunction and enhanced photocatalytic hydrogen evolution. Dalton Transactions, 2020, 49, 10816-10823.	1.6	28
51	Rapid magnetic solidâ€phase extraction of Congo Red and Basic Red 2 from aqueous solution by ZIFâ€8@CoFe 2 O 4 hybrid composites. Journal of Separation Science, 2016, 39, 3647-3654.	1.3	27
52	Adsorption behavior of methylene blue on Fe <sub>3</sub> O <sub>4</sub> -embedded hybrid magnetic metal–organic framework. Desalination and Water Treatment, 2016, 57, 25216-25225.	1.0	27
53	The biological performance of cell-containing phospholipid polymer hydrogels in bulk and microscale form. Biomaterials, 2010, 31, 8839-8846.	5.7	26
54	Fabrication of nanocomposites composed of silver cyanamide and titania for improved photocatalytic hydrogen generation. Dalton Transactions, 2015, 44, 19948-19955.	1.6	25

#	Article	IF	CITATIONS
55	Hierarchical spinel Ni Co1-Fe2O4 microcubes derived from Fe-based MOF for high-sensitive acetone sensor. Ceramics International, 2018, 44, 19390-19396.	2.3	25
56	Synergetic Effect of Tetraethylammonium Bromide Addition on the Morphology Evolution and Enhanced Photoluminescence of Rare-Earth Metal–Organic Frameworks. Inorganic Chemistry, 2020, 59, 14318-14325.	1.9	24
57	Morphology controlled synthesis of Ba4Bi3F17:Er3+,Yb3+ and the dual-functional temperature sensing and optical heating applications. Journal of Alloys and Compounds, 2020, 844, 156116.	2.8	24
58	Highly sensitive and selective triethylamine gas sensor based on hierarchical radial CeO2/ZnO n-n heterojunction. Sensors and Actuators B: Chemical, 2022, 367, 132031.	4.0	24
59	Synergetic effect of Fe2O3 and BiVO4 as photocatalyst nanocomposites for improved photo-Fenton catalytic activity. Journal of Materials Science, 2019, 54, 8236-8246.	1.7	22
60	Hierarchical hollow BiFeO <sub>3</sub> microcubes with enhanced acetone gas sensing performance. Dalton Transactions, 2021, 50, 6702-6709.	1.6	22
61	Design optimization of CsPbBr <sub>3</sub> nanocrystals into zeolite Beta composites as ultra-stable green emitters for backlight display applications. Journal of Materials Chemistry C, 2021, 9, 12118-12123.	2.7	22
62	Cu-bearing high-entropy alloys with excellent antiviral properties. Journal of Materials Science and Technology, 2021, 84, 59-64.	5.6	22
63	Rational design of direct Z-scheme heterostructure NiCoP/ZIS for highly efficient photocatalytic hydrogen evolution under visible light irradiation. Separation and Purification Technology, 2021, 275, 119153.	3.9	22
64	SALEâ€Ing a MOFâ€Based "Ship of Theseus.―Sequential Buildingâ€Block Replacement for Complete Reformulation of a Pillaredâ€Paddlewheel Metalâ€Organic Framework. European Journal of Inorganic Chemistry, 2016, 2016, 4345-4348.	1.0	21
65	Fabrication of ternary polyaniline-graphene oxide-TiO2 hybrid films with enhanced activity for photoelectrocatalytic hydrogen production. Separation and Purification Technology, 2018, 193, 358-367.	3.9	21
66	Hierarchical Zn1-xCdxS microclusters with superior visible-light-driven photocatalytic hydrogen generation performance. Journal of Alloys and Compounds, 2019, 809, 151869.	2.8	21
67	Fabrication of AgI/MILâ€53(Fe) Composites with Enhanced Photocatalytic Activity for Rhodamine B Degradation under Visible Light Irradiation. Applied Organometallic Chemistry, 2018, 32, e4325.	1.7	20
68	Immobilization of cellulase proteins on zeolitic imidazolate framework (ZIF-8)/polyvinylidene fluoride hybrid membranes. New Journal of Chemistry, 2018, 42, 17429-17438.	1.4	20
69	A microcube-like hierarchical heterostructure of α-Fe <sub>2</sub> O <sub>3</sub> @α-MoO <sub>3</sub> for trimethylamine sensing. Dalton Transactions, 2020, 49, 8114-8121.	1.6	20
70	Controlled synthesis of Bi <sub>2</sub> O <sub>3</sub> /BiOBr/Zn <sub>2</sub> GeO <sub>4</sub> heterojunction photocatalysts with enhanced photocatalytic activity. Journal of the American Ceramic Society, 2018, 101, 5858-5869.	1.9	19
71	Selective adsorption of malachite green (MG) and fuchsin acid (FA) by ZIF-67 hybridized polyvinylidene fluoride (PVDF) membranes. Dalton Transactions, 2021, 50, 8927-8937.	1.6	19
72	Improved stability of all-inorganic perovskite nanocrystals in hierarchical ZSM-5 zeolites for multimodal applications. Chemical Engineering Journal, 2022, 437, 135290.	6.6	19

#	Article	IF	CITATIONS
73	Hierarchical magnetic BiFeO3 microcages: Controlling synthesis and visible-light photocatalytic activity. Ceramics International, 2019, 45, 1554-1561.	2.3	18
74	Yolk–shell (Cu,Zn)Fe <sub>2</sub> O <sub>4</sub> ferrite nano-microspheres with highly selective triethylamine gas-sensing properties. Dalton Transactions, 2020, 49, 14475-14482.	1.6	18
75	The Hydrothermal Synthesis and Crystal Structure of (H2O)[Ge5O10] and [(CH3)4N][Ge10O20OH], Two Novel Porous Germanates. Chemistry Letters, 2004, 33, 74-75.	0.7	17
76	BiOBr-assisted hydrothermal synthesis of hierarchical Bi <sub>4</sub> (GeO <sub>4</sub> ) <sub>3</sub> /Zn <sub>2</sub> GeO <sub>4</sub> microspheres for optical sensor application. Journal of Materials Chemistry C, 2018, 6, 9778-9785.	2.7	17
77	Dual-emissive Eu3+, Tb3+ co-doped Gd2(MoO4)3 phosphor for optical thermometry application. Journal of Physics and Chemistry of Solids, 2021, 153, 110032.	1.9	17
78	Fabrication of organic–inorganic hybrid membranes composed of poly(vinylidene fluoride) and silver cyanamide and their high photocatalytic activity under visible light irradiation. RSC Advances, 2016, 6, 61920-61926.	1.7	16
79	Ag <sub>3</sub> PO <sub>4</sub> â€MILâ€53(Fe) Composites with Visibleâ€Lightâ€Enhanced Photocatalytic Activities for Rhodamine B Degradation. ChemistrySelect, 2018, 3, 8045-8050.	0.7	16
80	Optimizing electronic structure and charge transport of sulfur/potassium coâ€doped graphitic carbon nitride with efficient photocatalytic hydrogen evolution performance. Applied Organometallic Chemistry, 2019, 33, e5163.	1.7	16
81	CdS/Ag <sub>2</sub> S/g-C <sub>3</sub> N <sub>4</sub> ternary composites with superior photocatalytic performance for hydrogen evolution under visible light irradiation. Dalton Transactions, 2021, 50, 3253-3260.	1.6	16
82	Surface functionalization of zirconium dioxide nano-adsorbents with 3-aminopropyl triethoxysilane and promoted adsorption activity for bovine serum albumin. Materials Chemistry and Physics, 2016, 176, 129-135.	2.0	15
83	An improved carbothermal process for the synthesis of fine-grained boron carbide microparticles and their photoelectrocatalytic activity. Ceramics International, 2018, 44, 1052-1058.	2.3	15
84	Nickel Nanoparticles Encapsulated in Microporous Graphenelike Carbon (Ni@MGC) as Catalysts for CO <sub>2</sub> Methanation. Industrial & Engineering Chemistry Research, 2019, 58, 20536-20542.	1.8	15
85	Ag2CO3-derived Ag/g-C3N4 composite with enhanced visible-light photocatalytic activity for hydrogen production from water splitting. International Journal of Hydrogen Energy, 2020, 45, 20851-20858.	3.8	15
86	Fast synthesis of SSZ-13 zeolite by steam-assisted crystallization method. Microporous and Mesoporous Materials, 2020, 293, 109789.	2.2	14
87	Ionothermal synthesis of a photochromic inorganic–organic complex for colorimetric and portable UV index indication and UVB detection. RSC Advances, 2020, 10, 41720-41726.	1.7	14
88	Perovskite Multiple Quantum Wells on Layered Materials toward Narrow-Band Green Emission for Backlight Display Applications. ACS Applied Materials & Interfaces, 2020, 12, 27386-27393.	4.0	14
89	Combining solvent-assisted linker exchange and transmetallation strategies to obtain a new non-catenated nickel (II) pillared-paddlewheel MOF. Inorganic Chemistry Communication, 2016, 67, 60-63.	1.8	13
90	Lipase immobilization on UiO-66/poly(vinylidene fluoride) hybrid membranes and active catalysis in the vegetable oil hydrolysis. New Journal of Chemistry, 2020, 44, 14379-14388.	1.4	12

#	Article	IF	CITATIONS
91	Facile synthesis of accordion-like Y2O3:Er3+ nanothermometers for ratiometric temperature sensing applications. Journal of Luminescence, 2020, 223, 117207.	1.5	12
92	Nanosized CuO encapsulated Ni/Co bimetal Prussian blue with high anti-interference and stability for electrochemical non-enzymatic glucose detection. Dalton Transactions, 2021, 50, 13748-13755.	1.6	12
93	Quaternary Ammonium-Mediated Delamination of Europium-Based Metal–Organic Framework into Ultrathin Nanosheets for the Selective Photoelectrochemical Sensing of Fe <sup>3+</sup> . Inorganic Chemistry, 2021, 60, 19044-19052.	1.9	12
94	Rational design of Ag nanoparticles on ZIF-67-functionalized carbon nanotube for enzymeless glucose detection and electrocatalytic water oxidation. Journal of Alloys and Compounds, 2022, 910, 164878.	2.8	12
95	Two-step <i>in situ</i> synthesis of CsPbX <sub>3</sub> @TS-1 zeolite (X = Cl, Br, I) nanocomposites for optical thermometric, latent fingerprints and anti-counterfeiting applications. Materials Chemistry Frontiers, 2021, 5, 7843-7851.	3.2	11
96	Photocatalytic active silver organic framework: Ag(I)â€MOF and its hybrids with silver cyanamide. Applied Organometallic Chemistry, 2020, 34, e5972.	1.7	10
97	Preparation of Zn2GeO4 nanosheets with MIL-125(Ti) hybrid photocatalyst for improved photodegradation of organic pollutants. Materials Research Bulletin, 2021, 133, 111013.	2.7	10
98	[Ge9O14(OH)12](C6N2H16)2�H2O: A Novel Germanate with Ge?O Helical Chains Formed by Hydrothermal Synthesis that Can Separatetrans andcis Isomers in Situ. European Journal of Inorganic Chemistry, 2004, 2004, 4547-4549.	1.0	9
99	Germanate with Three-Dimensional 12 × 12 × 11-Ring Channels Solved by X-ray Powder Diffraction with Charge-Flipping Algorithm. Inorganic Chemistry, 2013, 52, 10238-10244.	1.9	9
100	Ratiometric fluorescence determination of hydrogen peroxide using carbon dot-embedded Ag@EuWO4(OH) nanocomposites. Mikrochimica Acta, 2020, 187, 369.	2.5	9
101	Synergistic adsorption and photocatalytic degradation of persist synthetic dyes by capsule-like porphyrin-based MOFs. Nanotechnology, 2021, 32, 465705.	1.3	9
102	Hierarchical spinel-type corn-like MGa2O4 (M = Ni, Co) architectures for selective triethylamine gas sensors. Materials Science in Semiconductor Processing, 2021, 133, 105993.	1.9	9
103	(C4N2H12)(NH4)2[(GeO2)3(GeO1.5F3)2]: A new layered germanate containing helical arrays of H-bond. Inorganic Chemistry Communication, 2011, 14, 1842-1845.	1.8	8
104	How to fit a response current-concentration curve? A semi-empirical investigation of non-enzymatic glucose sensor based on PANI-modified nickel foam. Journal of Electroanalytical Chemistry, 2019, 840, 384-390.	1.9	8
105	Flocculent VS nanoparticle aggregate-modified NiCo <sub>2</sub> S <sub>4</sub> nanograss arrays for electrocatalytic water splitting. Sustainable Energy and Fuels, 2021, 5, 3858-3866.	2.5	8
106	Fabrication of PVDF membranes entrapped with oleic acid modified TiO2 and selective adsorption toward bovine hemoglobin. RSC Advances, 2015, 5, 48607-48614.	1.7	7
107	Preparation and dual sensing property of Zn2GeO4:Mn2+@ZIF-8 heterostructure chemosensor. Materials Letters, 2018, 210, 235-238.	1.3	7
108	Morphology-controllable synthesis of hierarchical hollow GaFeO3 microcubes with selective triethylamine gas-sensing properties. Ceramics International, 2022, 48, 4554-4562.	2.3	7

#	Article	IF	CITATIONS
109	Distribution of trivalent metal cations in alumino-/gallogermanate zeolites with JST topology. Dalton Transactions, 2012, 41, 12170.	1.6	6
110	Effects of solventâ€induced morphology evolution of Zn <sub>2</sub> GeO <sub>4</sub> on photocatalytic activities of g <sub>3</sub> N <sub>4</sub> /Zn <sub>2</sub> GeO <sub>4</sub> composites. Journal of the American Ceramic Society, 2019, 102, 6517-6528.	1.9	6
111	Dual cocatalysts decorated three dimensionally ordered mesoporous gâ€C <sub>3</sub> N <sub>4</sub> with homogeneous wall thickness for enhanced photocatalytic performance. Applied Organometallic Chemistry, 2020, 34, e5552.	1.7	6
112	Fabrication of polyaniline-supported bimetal AgNi nanoparticles and the enhanced performance towards formate oxidation. Journal of Solid State Electrochemistry, 2021, 25, 1197-1205.	1.2	6
113	A family of germanates constructed from Ge <sub>7</sub> clusters co-templated by metal complexes and organic/inorganic species. CrystEngComm, 2014, 16, 9545-9554.	1.3	5
114	Nickel Ammine Complexâ€derived NiO Modified g  3 N 4 Composites with Enhanced Visibleâ€light Photocatalytic H 2 Evolution Performance. ChemistrySelect, 2019, 4, 8095-8103.	0.7	5
115	Microwave-assisted synthesis of a thermally stable Zn-containing aluminophosphate with ERI-zeotype structure templated by diquaternary alkylammonium. RSC Advances, 2014, 4, 49846-49849.	1.7	4
116	Oxygen sensitive electrospun nanofibers doped with rare earth complexes: Characterization and performance. Optical Materials, 2022, 125, 112099.	1.7	4
117	Hydrogen bonding-mediated assembly of carbon dot@Zr-based metal organic framework as a multifunctional fluorescence sensor for chlortetracycline, pH and temperature detection. New Journal of Chemistry, 2022, 46, 13021-13029.	1.4	4
118	Test-strip and smartphone-assisted Eu-TCPE-based ratiometric fluorescence sensor for the ultrasensitive detection of tetracycline. New Journal of Chemistry, 2022, 46, 13129-13136.	1.4	4
119	Synthesis and structural characterization of three 3-D aluminogermanates with different topologies. CrystEngComm, 2014, 16, 5103-5109.	1.3	3
120	Preparation of ZIF-8 nanoparticle-decorated Zn2GeO4 nanorods with high photocatalytic performance for chromium (VI) reduction. , 0, 106, 200-208.		3
121	A hierarchical hollow Ni/Co-functionalized MoS <sub>2</sub> architecture with highly sensitive non-enzymatic glucose sensing activity. Dalton Transactions, 2021, 50, 10059-10066.	1.6	2
122	Dual-emitting ZIF-8⊃4-MU@Zn2GeO4:Mn2+ nanocomposites for ratiomertic luminescent thermometer and information encryption. Dyes and Pigments, 2022, 205, 110522.	2.0	2
123	Copper and iron mediated growth of surfactantâ€free PtCu and PtFe advanced electrocatalysts for water oxidation and oxygen reduction. Electrochemical Science Advances, 0, , e2100033.	1.2	1
124	Cell-Compatible Hydrogels: A Microfluidic Hydrogel Capable of Cell Preservation without Perfusion Culture under Cell-Based Assay Conditions (Adv. Mater. 28/2010). Advanced Materials, 2010, 22, n/a-n/a.	11.1	0
125	L-lysine-assisted hydrothermal synthesis of β-NaGdF4:Eu3+ microcrystals: Morphology evolution, luminescence and magnetic properties. Surfaces and Interfaces, 2021, 22, 100851.	1.5	0
126	Solvent-free synthesis of hierarchical Tb3+-doped Yttrium benzene-1,3,5-tricarboxylate metal organic framework nanosheets for fast and highly sensitive fluorescence detection of Fe3+ and Cr2O72â'' ions. , 2022, , .		0